Structural optimisation based on the boundary element and level set methods

B.Ullah*, J.Trevelyan, P.C.Matthews

School of Engineering and Computing Sciences, Durham University, South Road, Durham DH1 3LE, UK.

Abstract

A new method of structural topology optimisation is proposed in which an evolutionary approach is used with boundary element and level set methods. During the optimisation iterations, the proposed method automatically introduces internal cavities and does not rely on an initial guess topology with pre-existing holes. The zero level set contours describing both the external geometry and the internal cavities are converted to non-uniform rational B-splines (NURBS) for smooth boundary element meshing at each iteration. The optimal geometries generated by the proposed method for two-dimensional cases closely resemble to those available in the literature for a range of benchmark examples in the field of topology optimisation.

Keywords: structural optimisation, boundary element method, level set method, NURBS

*Corresponding author

Email addresses: baseer.ullah@durham.ac.uk (B.Ullah), jon.trevelyan@durham.ac.uk (J.Trevelyan), p.c.matthews@durham.ac.uk (P.C.Matthews)

1. Introduction

Structural engineers worldwide are driven by the search for a design that is in some sense optimal, making the most efficient use of materials. In order to support this search, an extensive body of literature has appeared over the last decades describing various numerical techniques to generate structures that are optimal in terms of quantities such as weight, cost and stiffness. Most schemes in the literature make use of the finite element method (FEM) to perform the structural analysis that guides the optimisation process. Methods that have enjoyed enduring popularity include the homogenisation method of Bendsøe and Kikuchi [1], based on varying the material porosity. This was enhanced to improve the stability for practical usage with the development of the SIMP method by Rozvany *et al.* [2].

The most challenging structural optimisation problems are those of topology optimisation, which remains an active research area. Eschenauer *et al.* [3] introduced the bubble method, which is based on the insertion of new holes in the structure and the subsequent use of a shape optimisation method to determine their optimal size and shape. The concept of adaptive topology optimisation, developed by Maute and Ramm [4], is based on the smoothness of the effective design space with a cubic or Bézier spline approximation based on the density distributions. This procedure not only reduces the number of design variables but also provides smooth geometry. Papalambros and Chirehdast [5] presented a three phase, homogenisation-based approach to integrated structural optimisation with CAD.

The inspiration from nature, i.e. how structures such as bones, trees and shells achieve their optimum over a period of time under specific envi-

ronmental conditions, led to the development of the evolutionary structural optimisation (ESO) method. The simple evolutionary method presented by Xie and Steven [6] progressively removes material (i.e. finite elements) from low stress regions based on some rejection criteria. Similarly in Bi-directional ESO [7, 8], material removal is accompanied by material addition in highly stressed regions. Garcia and Steven [9] introduced the concept of Fixed Grid (FG) FE analysis to simplify the meshing in order to enhance computational efficiency in problems where geometry changes with time. This is attractive from the point of view of efficiency, but the accuracy of stresses in elements intersecting the problem boundaries may become compromised. Dunning *et al.* [10] have used FG-FE simulations to drive a sensitivity based scheme for topology optimisation in the presence of uncertainty in the loading.

There has been some controversy over the last decade over the validity of ESO as an optimisation approach when the removal and addition of material is provoked by local stress values, in contrast with the use of design sensitivities related to an objective function. In spite of this, stress based ESO schemes have remained popular on account of their simplicity and extensive empirical evidence of the fact that their optimal solutions closely resemble those derived by more rigorous descent methods (e.g. Li *et al.* [11]).

While finite elements have been a popular method, they have some shortcomings when used as the analysis engine for optimisation methods. Haftka and Grandhi [12] highlighted the principal issue in shape optimisation, that it is difficult to ensure the accuracy of the analysis for a continuously changing finite element model; the change in the shape of a structure distorts the shape of the finite elements, with consequent deterioration in the accuracy of

the stress solution. For these reasons it has been popular to use fixed grid FE approaches [9] to reduce distortion. However, poorly shaped elements still remain. The requirement of a smooth optimal geometry further increases the computational cost due to high mesh refinement at the boundaries. This leads us to propose the boundary element method (BEM) as an appealing alternative. The BEM is a well-established alternative to the FEM in structural analysis, and is attractive because it requires discretisation only at the structural boundary. This reduction of problem dimensionality considerably simplifies the re-meshing task, which can be performed efficiently and robustly. Thus, its rapid and robust re-meshing and accurate boundary stress solutions make the BEM a natural choice in the field of shape and topology optimisation.

While the BEM has been exploited for structural optimisation in earlier works [13, 14, 15] it is topology optimisation on which this paper focusses. Cervera and Trevelyan [16, 17] used BEM for topology optimisation of two and three dimensional problems. In their ESO approach the moving geometry of the structure was represented by NURBS [18] explicitly, the spline control points being moved in response to local stress values. The boundary element based topological derivatives concept was used for the first time by Marczak [19] for the topology optimisation of thermally conducting solids. The proposed formulation was based on the concept of introducing an iterative material removal procedure in a BEM framework. Carretero and Cisilino [20] presented topology optimisation of 2D elastic structures using the BEM with linear elements, inserting small holes in the model around internal points with the lowest values of the topological derivative. Bertsch

et al. [21] presented three dimensional elastic topology optimisation in a BEM framework with the topological shape sensitivity method for the direct calculation of topological derivatives from stress fields.

The Level Set Method (LSM) presented by Osher and Sethian [22] has emerged as a powerful tool for describing the evolution of moving boundaries. It is particularly powerful in its ability to deal with complex merging and separation of different boundaries. There have been several examples in the literature of researchers exploiting this in topology optimisation, firstly by Sethian and Wiegmann [23] and later Wang *et al.* [24]. Numerical shape derivatives were used by Allaire *et al.* [25] for structural optimisation in 2D and 3D with both linear and nonlinear elasticity models. However, their approach is restrictive in that no new holes can be nucleated in 2D structural optimisation; moreover, the optimum solution is highly dependent on the initially guessed topology. Allaire and Jouve [26] combined the shape derivatives with topological derivatives to present a level set based optimisation method capable of automatic hole insertion. The proposed approach was shown to be independent from local minima but the implementation of topological derivatives is very difficult in numerical practice [27, 28] because, the hole size is dependent on a single mesh cell which cannot be infinitesimally small as proposed in the method [26]. In addition, the resulting optimal structure depends on the values of various parameters which can affect the stability of the optimisation process [29]. Other examples of LSM combination with FEM-based structural optimisation schemes can be found in [29, 30, 31].

The use of BEM with the level set method in structural optimisation was first used by Abe *et al.* [32]. During each optimisation iteration the evolving

structural boundary is re-constructed from the zero level set contours, which consists of line segments joining the zero level set intersection points. The resulting non-smooth geometry is then meshed with linear boundary elements to perform the sensitivity analysis for the next iteration. The non smooth geometry and the linear boundary elements greatly reduce the accuracy of the expensive sensitivity calculations, and hence the method requires a large number of iterations to achieve convergence. In addition the use of sensitivity analysis restricts the nucleation of new holes and makes this method highly dependent on the initially guessed topology.

This paper presents an initial study of the integration of BEM, evolutionary optimisation approach, LSM and NURBS for 2D structural optimisation problems. The proposed method uses the 2D version of the BEM analysis software Concept Analyst (**CA**) [33]. The approach overcomes many of the shortcomings of earlier works; boundaries remain smooth throughout, and holes are inserted automatically revealing the final topology from a simple starting geometry. This paper is organised as follows. The basic details of LSM are introduced in Section 2, and the BEM is developed in Section 3. In Section 4 we present the details of the optimisation algorithm and its implementation. The results obtained from the proposed algorithm are presented and discussed in Section 5, and the paper closes with some concluding remarks in Section 6.

2. Level Set Method

The LSM is an efficient numerical technique developed by Osher and Sethian [22] for the tracking of propagating interfaces. The wide variety

of applications in which LSM is successfully implemented include computer vision, medical scans, seismic analysis, fluid flow, structural optimisation and optimal control. The propagation of the structure boundary during the optimisation can be linked with the evolution of the function ϕ as an initial value problem. This means that the position of the structure boundary at any time t is given by the zero level set function ϕ. Therefore the evolution equation of the LSM given in [22] is

$$\frac{\partial \phi}{\partial t} + F|\nabla \phi| = 0 \tag{1}$$

where F is the velocity in the normal direction and t is the virtual time.

In the implicit representation the connectivity of the discretisation does not need to be determined explicitly. This is one of the most interesting features of the implicit geometric representation, in that merging and breaking of curves in 2D and surfaces in 3D can be handled automatically. Thus in this work the holes appear, merge and vanish automatically. It is worth mentioning that, although we are not solving time-dependent problems, the LSM uses virtual time to describe the advancing front.

The implicit method uses the Eulerian approach to represent an evolving geometry. In 2D this method works on an underlying fixed Cartesian grid. The geometry of the structure to be optimised is embedded as the zero level set of a higher dimensional function ϕ. The value of ϕ is the distance of a particular grid point from the boundary with a sign to indicate points either inside or outside of the boundary. We define Ω^- as the region contained within the boundary, Ω^+ as the union of the regions inside holes and the region of the design domain outside the boundary, and the contour $\partial\Omega$ as the interface between the non-overlapping regions Ω^- and Ω^+. These definitions

are expressed as follows and shown in Figure 1.

$$\phi(\vec{x}) \begin{cases} < 0 & \vec{x} \in \Omega^- \\ = 0 & \vec{x} \in \partial\Omega \\ > 0 & \vec{x} \in \Omega^+ \end{cases} \tag{2}$$

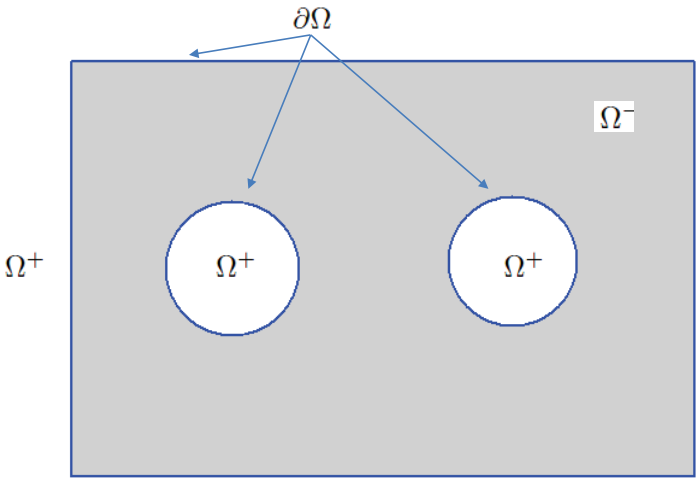

Figure 1: Geometry implicit representation

3. Boundary Element Method

The Boundary Element Method (BEM) is a standard technique for computational solution of partial differential equations. There are numerous textbooks describing the method (e.g. Becker [34]), but for completeness a brief description is included in this section.

We consider linear elasticity in the domain $\Omega^- \subset \mathbb{R}^2$, having boundary $\partial\Omega = \Gamma$. The boundary includes an exterior boundary and may contain

interior boundaries to model holes in the structure. These will be important as design topologies develop. We solve the equilibrium equations

$$\sigma_{ij,j}(\vec{x}) + b_i(\vec{x}) = 0, \qquad \vec{x} \in \Omega^- \tag{3}$$

where $i, j = x, y$, the problem being subject to boundary conditions

$$u_i(\vec{x}) = \bar{u}, \qquad \vec{x} \in \Gamma_u \tag{4}$$

$$t_i(\vec{x}) = \bar{t}, \qquad \vec{x} \in \Gamma_t \tag{5}$$

In the above, u_i represents a displacement component, σ the Cauchy stress tensor and b the body force vector. We define $\Gamma = \Gamma_u \cup \Gamma_t$, but since it is commonplace in practice to prescribe different boundary condition types in different coordinate directions at the same point, this definition is purely symbolic. The traction component, t_i, is given by

$$t_i(\vec{x}) = \sigma_{ij}(\vec{x}) n_j(\vec{x}), \qquad \vec{x} \in \Gamma \tag{6}$$

where n is the unit outward pointing normal vector at $\vec{x}$. The terms $\bar{u}, \bar{t}$ are prescribed known displacements and tractions respectively. The Einstein summation convention is assumed throughout. Taking for simplicity here the case $b = 0$, the differential equations (3) can be transformed into an equivalent integral equation form known as the Somigliana identity. We may write

$$c_{ij}(\vec{x}) u_j(\vec{x}) + \fint_\Gamma T_{ij}(\vec{x}, \vec{y}) u_j(\vec{y}) d\Gamma(\vec{y}) = \int_\Gamma U_{ij}(\vec{x}, \vec{y}) t_j(\vec{y}) d\Gamma(\vec{y}) \tag{7}$$

where T_{ij}, U_{ij} are respectively the traction and displacement kernels, or fundamental solutions. The free coefficients, c_{ij}, arise from the strong singularity

in the integral containing the traction kernel; this integral is denoted $\oint$ to indicate its evaluation in the Cauchy Principal Value sense. The boundary may be discretised using elements, i.e.

$$\Gamma = \bigcup_{e=1}^{N_e} \Gamma_e, \quad \Gamma_i \cap \Gamma_j = \emptyset, i \neq j \tag{8}$$

and the geometry of each element parameterised in terms of a local intrinsic coordinate $\xi^e \in [-1, 1], e = 1, ..., N_e$, allowing (7) to be rewritten

$$\begin{aligned} c_{ij}(\vec{x})u_j(\vec{x}) + \sum_{e=1}^{N_e}\sum_{l=1}^{m}\left[\int_{-1}^{+1} T_{ij}(\vec{x}, \vec{y}(\xi^e))N_l(\xi^e)J^e(\xi^e)\, d\xi^e\right] u_j^{el} \\ = \sum_{e=1}^{N_e}\sum_{l=1}^{m}\left[\int_{-1}^{+1} U_{ij}(\vec{x}, \vec{y}(\xi^e))N_l(\xi^e)J^e(\xi^e)\, d\xi^e\right] t_j^{el} \end{aligned} \tag{9}$$

where l is a local node number, on element e, that varies from 1 to $m = 2, 3, ...$ for linear, quadratic elements etc., $\vec{y}$ is the location on the element corresponding to the variable of integration ξ^e, N_l is the Lagrangian shape function for node l, $J^e = d\Gamma_e/d\xi^e$ is the Jacobian of transformation and u_j^{el} and t_j^{el} are displacements and tractions, respectively, at local node l on element e. Taking point $\vec{x}$ to be a node point, and evaluating the boundary integrals in (9) using a suitable scheme that copes with the singularities in the fundamental solutions, we arrive at

$$c_{ij}(\vec{x})u_j(\vec{x}) + \sum_{e=1}^{N_e}\sum_{l=1}^{m} h^{el}u_j^{el} = \sum_{e=1}^{N_e}\sum_{l=1}^{m} g^{el}t_j^{el} \tag{10}$$

where h^{el}, g^{el} are the evaluated integrals. Finally, placing point $\vec{x}$ at each node in turn, equations of this form may be developed at each, and these may be assembled to form a linear system

$$[\mathbf{H}]\{\mathbf{u}\} = [\mathbf{G}]\{\mathbf{t}\} \tag{11}$$

where the matrices **H** and **G** contain the coefficients h_{el} and g^{el} respectively, and multiply vectors of nodal displacements and tractions. Application of the boundary conditions (4) and (5) reduces the problem to a square system that can be solved for unknown boundary displacements and tractions.

It is important in topology optimisation to determine accurate solutions at *internal points*, i.e. points $\vec{x} \in \Omega^{-} \backslash \Gamma$. Once equation (11) has been solved, internal point displacements can be found using (9) by taking $\vec{x}$ as the point in question and letting $c_{ij} = \delta_{ij}$, where δ_{ij} is the Kronecker delta, and likewise stress components may be determined from a differentiated form of the same expression.

4. Optimisation Algorithm

The present research work focuses on the integration of a stress based optimisation approach with the BEM as a structural analysis tool, the LSM as a numerical technique for handling the complex geometry changes and NURBS as a modeling tool to convert the non-smooth level sets updated geometry into a standard CAD representation. The main steps in this optimisation process are summarised as follows:

1. Define structural geometry with applied loads and constraints.
2. Initialize level set grid with signed distance function.
3. Carry out boundary element analysis.
4. Insert holes in the structure based on the hole insertion criterion.
5. Identify high and low stress boundary nodes based on the material addition and removal criterion and assign positive speed values to high

stress boundary nodes, while negative speed values to the low stress boundary nodes.

6. Solve the level set equation based on the speed values assigned in step 5 to evolve the topology of the structure.
7. Trace the zero level set contours and convert them into a standard CAD representation i.e. NURBS.
8. Repeat the above procedure from step 3, until the stopping criterion is satisfied.

The implementation of the above optimisation algorithm is shown in Figure 2 and discussed in the following sections in detail. Many of these steps involve criteria of various types involving the comparison of stresses, volumes, etc. against various coefficients. These have been developed through extensive numerical testing on a range of optimisation problems.

4.1. Structure geometry, loading and constraints

In the first step of this optimisation method loading and constraints are applied to a given structure which needs to be optimised. The geometry of this initial structure is arbitrary, and is defined as a polygon in which each edge is a line segment which may be straight or curved. In most research work of this type, the initial geometry is a simple rectangle. For explanation of various portions of the structural geometry, the example of a cantilever beam is shown in Figure 3. The line segments describing portions of the boundary over which loads and constraints are prescribed, highlighted as red lines in Figure 3, remain fixed, while the remaining line segments are allowed to be modified during the optimisation process. The modifiable line segments

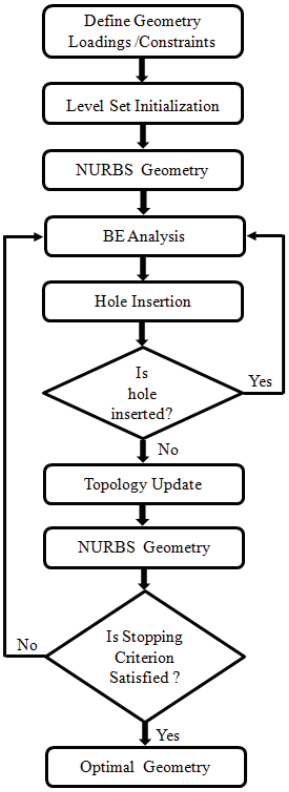

Figure 2: Optimisation flow chart

shown in Figure 3(a) are first converted into NURBS (Figure 3(b)) prior to the BEM structural analysis. The conversion details of line segments into NURBS are explained in Section 4.7. In this particular example there are three line segments and three NURBS segments shown in Figure 3(b).

We denote using V_0 the initial volume of the structure (this is interpreted as the area in a 2D representation).

4.2. Geometric update

The equivalent stress based criterion or von Mises criterion [11] is used for material removal and addition during the optimisation process. For clar-

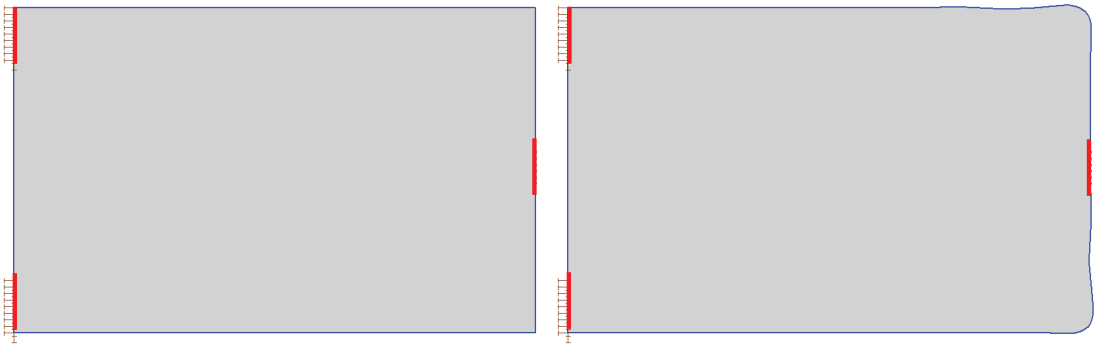

(a) Initial geometry (b) NURBS geometry

Figure 3: Defining structural geometry

ification we present the definition of von Mises stress, σ_{vm}, as

$$\sigma_{vm} = \frac{1}{\sqrt{2}}\sqrt{(\sigma_1 - \sigma_2)^2 + (\sigma_2 - \sigma_3)^2 + (\sigma_3 - \sigma_1)^2} \tag{12}$$

where σ_1, σ_2 and σ_3 are the principal stresses.

The optimisation method used in this research work is based on a bi-directional material approach, i.e. the material addition and removal takes place simultaneously during the optimisation iterations, which is equivalent to an evolutionary approach presented in [7]. The boundary element analysis calculates the von Mises stresses at each node of the structural boundary and at internal points inside the boundary. Inefficient material, which needs to be progressively removed, is identified as the regions in the locality of nodes satisfying

$$\sigma_{vm} < RR\sigma_{max} \tag{13}$$

where RR is the removal ratio and σ_{max} is the maximum von Mises stress in the initial design. Similarly regions where material should be added are identified as those in the locality of the boundary nodes with high stresses

satisfying

$$\sigma_{vm} > \min(\sigma_{max}, \sigma_y) \tag{14}$$

where σ_y is the material's yield stress. The initial removal ratio RR is 0.01, and this is increased by an incremental removal ratio RR_i (as shown in (15)) periodically as the optimisation progresses, when the combined volume of material experiencing $\sigma_{vm} < RR\sigma_{max}$ falls below a threshold of $0.4V$ (where V is the volume at the current iteration), until the stopping criterion is satisfied.

$$RR = RR + RR_i \tag{15}$$

The values of RR_i used are shown in each example in Section 5.

Material addition takes place by the outward movement of external boundary and the inward movement of internal boundaries (i.e. holes), while in the material removal process the external boundary is moved inward and the internal boundaries are moved outward. Material removal inside the structure takes place by inserting holes around the low stress internal points. These two steps of boundary movement and hole insertion are explained in detail in the following sub-sections.

4.2.1. Material removal and addition

The structural boundaries are modified during the optimisation process with the LSM. The LSM requires the velocity to be defined at each level set grid point. In this step only the boundary velocity is calculated; the velocity extension method explained in Section 4.4 is later used to extend the boundary velocities to the level set grid points. A relationship similar to that proposed by Sethian and Wiegmann [23] has been developed through

numerous numerical experiments, and is used to convert the von Mises stress σ_{vm} at each node point to the scaled velocity F, as depicted in Figure 4. The intervals shown in Figure 4 can be characterised in terms of σ_{vm}, RR, σ_y, and σ_{max}, as follows:

- $\sigma_{vm} \in [0, \sigma_{t1}] : \sigma_{t1} = 0.5RR\sigma_{max}\,, F = -1$
- $\sigma_{vm} \in [\sigma_{t1}, \sigma_{t2}] : \sigma_{t2} = 0.9RR\sigma_{max}\,, F \in [-1, 0]$
- $\sigma_{vm} \in [\sigma_{t2}, \sigma_{t3}] : \sigma_{t3} = 0.95\min(\sigma_{max}, \sigma_y)\,, F = 0$
- $\sigma_{vm} \in [\sigma_{t3}, \sigma_{t4}] : \sigma_{t4} = \min(\sigma_{max}, \sigma_y)\,, F \in [0, 1]$
- $\sigma_{vm} \in [\sigma_{t4}, \infty) : F = 1$

The inward movement of the boundary eliminates inefficient material from the structure where F is negative. Likewise, there is an outward movement for a positive F and no movement of the boundary where F is zero.

4.2.2. Hole insertion

Material can also be removed by inserting holes in the internal regions of the structure experiencing low stress. In a BEM analysis stresses within the structure are calculated at internal points. The CA software generates these points automatically using the following algorithm.

- Rings of internal points are defined around holes.
- Arcs of internal points are defined around fillets and re-entry corners.

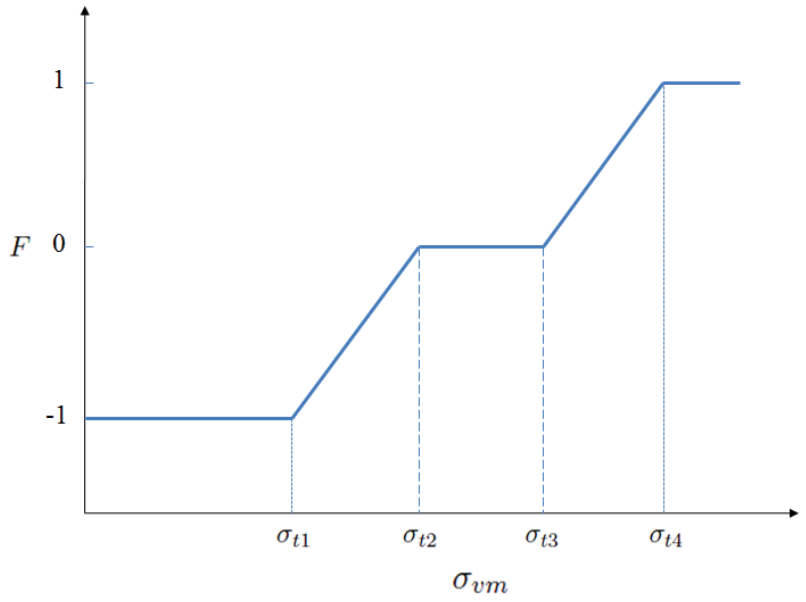

Figure 4: Algorithm for conversion of stress to scaled velocity F

- Lines of internal points are defined along possible neutral axis locations in bending.
- Remaining internal points, giving a total number equal to 1.5 × number of nodes,are placed randomly.
- A triangulation is generated from the 2D set of points (nodes and internal points).
- Laplacian smoothing is applied to the triangulation.
- Internal points too close to the boundary are repositioned.

The algorithm is designed to give smooth stress contours using a reasonable number of internal points (for computational efficiency) and has been refined

over many years' usage in academia and industry. The ability to produce smooth contours indicates that a sufficiently detailed description of the stress field is available for the optimization process. Although, these points are used to provide information for displaying stress contours, the von Mises stress at these points is also used to inform a criterion for hole insertion in the low stress regions in the structure. It should be noted that the procedure for defining the internal point locations includes some randomness. The main steps of this method are given below and for clarity also shown in Figure 5:

1. Identify internal points satisfying the following equation

$$\sigma_i \leq RR\sigma_{t1} \tag{16}$$

   where σ_i is the von Mises stress at a given internal point.
2. Sort the internal points identified in step 1 depicted with ■ in Figure 5(b) in ascending von Mises Stress order.
3. The first internal point, i.e. the least stressed internal point from the above step, is used as a centre depicted with ▲ in Figure 5(b) for the new hole.
4. Internal points satisfying a threshold stress level (related to Equation (16)) around the central point from step 2 are used to construct a convex polygon shown in Figure 5(c).
5. The vertices of the convex polygon are taken as control points to generate two NURBS curves to insert the new hole, as shown in Figure 5(d).
6. The above steps are repeated until there are no more internal points selected in step 1.

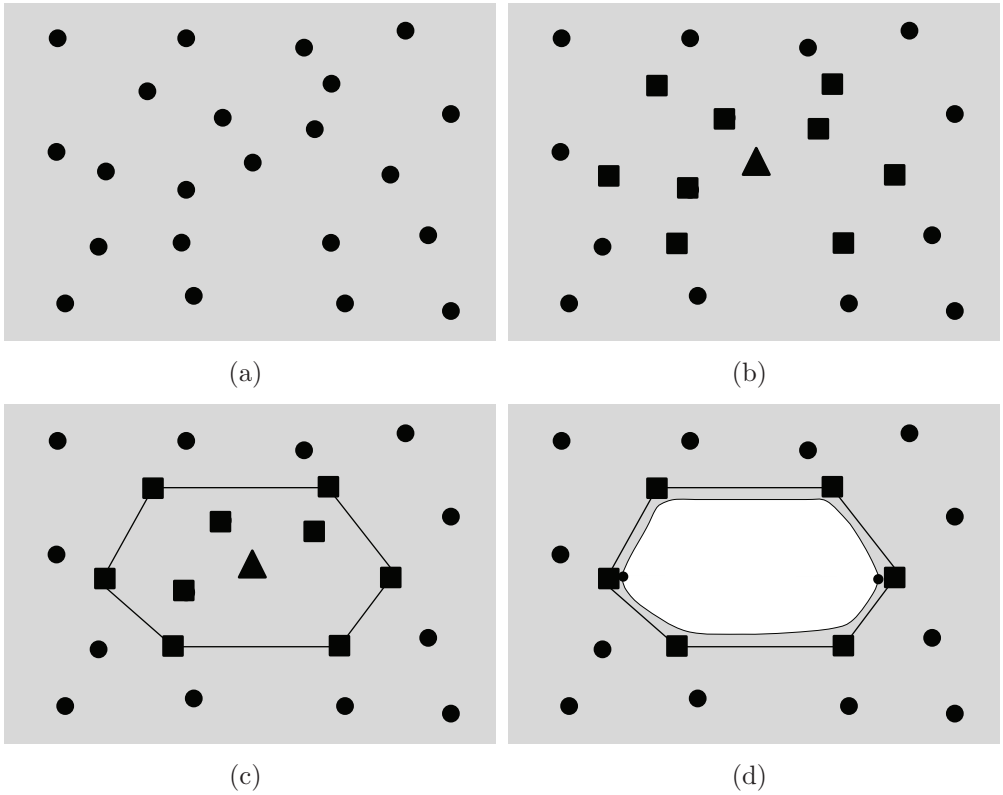

Figure 5: Creation of holes from internal points (• = internal points, ▲ = low stressed central internal point, ■ = low stressed internal points)

In situations when the number of internal points around the central point is less than 5, then no hole insertion takes place and the next internal point is used to repeat the above steps for hole insertion around it. The hole insertion changes the structural geometry, which is re-analyzed with BEM for the new stress distribution.

4.3. Level set initialization

The proposed algorithm adds and removes material during the optimisation process. The dimensions of the level set grid used in this algorithm are slightly bigger than the structural geometry, allowing for some enlargement of the design from the initial geometry. The use of NURBS geometry (see Section 4.7) provides the flexibility to use coarse and fine level set grids during the optimisation process. The approach of coarse and fine grids provides greater computational efficiency during the level set calculations. A coarse grid is used in the initial optimisation iterations, and the scheme switches to a finer grid once the volume has reduced to $0.35V_0$. The coarse and fine grids are defined using a grid spacing $d = 0.02D$ and $d = 0.01D$ respectively, where D is the largest dimension of the initial analysis model. In this initial study we have used both coarse and fine level set grids; for complex design domains and boundary conditions, a fine level set grid should be used throughout the optimisation iterations. The geometry defined in Section 4.1 is embedded as a higher dimensional function through signed distance calculations, and this initializes the level set grid. Re-initialization of the level set grid is carried out after each hole insertion and during the optimisation process to maintain the level set function as a signed distance (explained in detail in section 4.4).

4.4. Velocity extension

The velocity (calculated in Section 4.2.1) is now defined at the structural boundary. The LSM requires that the velocity should be defined not only for the zero level set but for the entire computational domain, which means that the boundary velocity should be extended to all grid points. But the velocity extension to all grid points is computationally expensive. Therefore

the velocity is only extended to the grid points in the narrow band around the boundary, using the methods developed by Adalsteinsson and Sethian ([35, 36]). The boundary segments with constraints and loads, are assigned with zero velocity before the velocity extension, this prevents these locations from movement during the optimisation process. The level set function is re-initialized by the substitution of the temporary signed distance function (computed during the velocity extension method) for the current level set function. This provides a very fast and accurate way of re-initialization of the level set function in the narrow band [37].

4.5. Update of level set function

After the velocity extension the level set Equation (1) is solved with an upwind finite difference approximation. The value of the time step for the solution of the level set equation is based on the Courant-Friedrichs-Lewy (CFL) condition. In each iteration, though, it is desirable to remove more material than the CFL condition permits. Therefore, in between each BEM simulation, multiple explicit time steps were used to update the level set function; this number decreases as the structure volume approaches the target volume. This is also a standard practice within the FEM based LSM optimisation methods [26]. During each optimisation iteration the number of times the level set function is updated depends on the volume fraction, which is defined as the structural volume at the current iteration, V, divided by the original volume V_0. In the initial iterations it is desirable that a larger fraction of the inefficient material is removed, so the level set function updates four times between each structural analysis. This is gradually reduced to a single update during the final stages of optimisation. The following scheme

has been developed through a series of numerical tests on a range of models.

- when $V > 0.9V_0$, four level set updates in each iteration
- when $0.8V_0 < V < 0.9V_0$, three level set updates in each iteration
- when $0.45V_0 < V < 0.8V_0$, two level set updates in each iteration
- when $V < 0.45V_0$, one level set update in each iteration

4.6. Zero level set contour tracing

The solution of the level set equation modifies the level set function ϕ based on the structural analysis results. The new zero level set contours are traced with an efficient contour tracing algorithm developed within the CA software. This algorithm linearly interpolates the positions of the zero level set points at the intersections with the level set grid lines. The contour tracing algorithm starts from calculating the position of a zero level set intersection point, and proceeds to follow the contour $\phi = 0$ by locating adjacent intersection points, stopping when the starting point is reached and a close contour has been defined. The algorithm terminates when there are no more zero level set contours to be traced in the computational domain. There are two advantages attached to this concept. The first is that only those grid cells are checked where the zero level set exists, thereby reducing the computational cost of checking all the grid cells. The second advantage is that the intersection points obtained are in a regular order, through which a closed contour can easily be constructed.

4.7. NURBS geometry

There are two options available to extract the updated geometry. For explanation purposes some portion of the level set grid is shown in Figure 6(a) and the positions of zero level set intersection points are shown in Figure 6(b). In the first option line segments are used to connect the zero level set intersection points (Figure 6(c)). This yields a non-smooth polygonal structural geometry with line segments of non-uniform length, especially when a coarse level set grid is being used. This geometry is required to be used in structural analysis in the next iteration. In the boundary element analysis if the zero level set intersection points are used directly as element nodal points (as in [32]), two intersection points can lie very close to each other (for example see Figure 6(c)), and this can cause difficulties and instabilities during the boundary element analysis. In addition the non-smoothness of the polygonal geometry can produce high stress concentrations, which can mislead the optimisation process. In order to overcome these difficulties the curve fitting techniques available in [18] are used to fit a single NURBS passing through the zero level set intersection points (see for example Figure 6(d)) for each of the modifiable segments of the structural geometry. This fitting technique provides flexibility of using coarse level set grid, which increases the computational efficiency of the optimisation algorithm. In this algorithm we used B-splines (a special case of NURBS) to represent the modifiable structural geometry segments. The fitted NURBS geometry (Figure 6(e)) is abstracted from the locations of the level set intersections. The automatic meshing facility in the CA software is used to define elements on each spline, using a setting which is designed to produce peak stresses to approximately

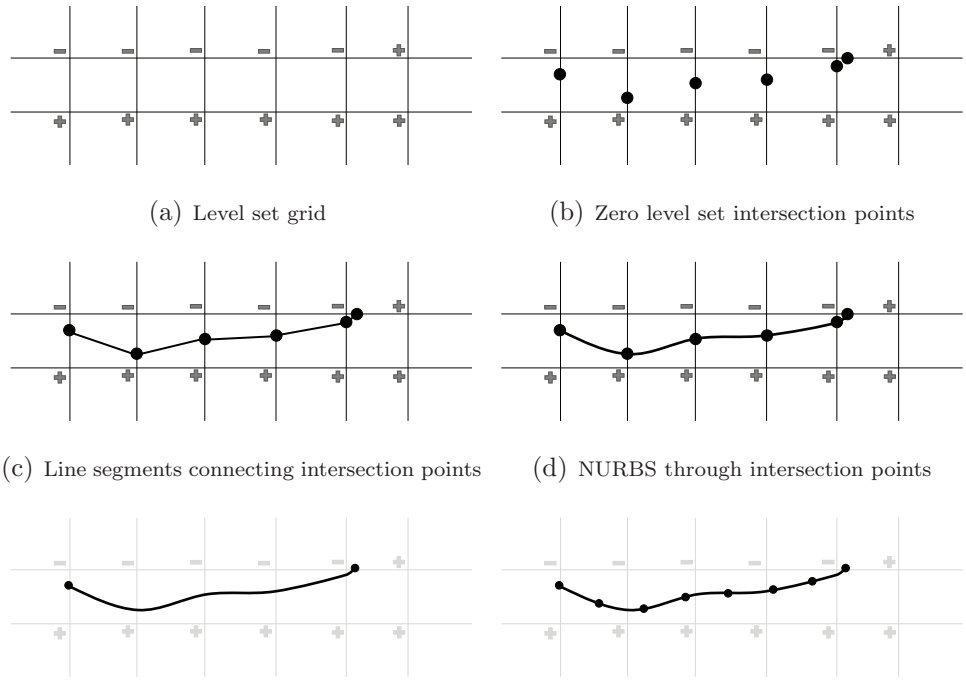

(a) Level set grid (b) Zero level set intersection points

(c) Line segments connecting intersection points (d) NURBS through intersection points

(e) NURBS (f) NURBS with BEM nodes

Figure 6: NURBS geometry

1% accuracy, either with uniformly distributed boundary element nodes as shown in Figure 6(f) or with grading as required for good BEM meshing practice. A linear elastic stress analysis is then automatically initiated. It should be noted that the boundary-only meshing naturally avoids problems of checkerboarding that are well known to require care in FEM optimisation schemes.

4.8. Performance indicator and stopping criterion

The idea to enhance the performance of a structure based on providing maximum possible stiffness against the applied loads is the basis of the

maximum stiffness criterion. However, simply seeking to maximise stiffness will lead to an increase in the weight of the structure, because the design space will become completely filled with material. In order to enhance the structural performance from both the stiffness and efficient material utilization points of view the concept of specific stiffness was developed [38], being defined as,

$$f_K = \frac{K}{V} \tag{17}$$

where K is the stiffness and V is the volume of the structure. In the case of multiple loads, it is difficult to find a clear definition of stiffness that can be used in this fashion. Thus we may use an equivalent concept, i.e. the specific strain energy, f_U, which is the product of strain energy U and the volume V of the structure [16], i.e.

$$f_U = UV \tag{18}$$

It is useful to monitor the reduction in f_U as a performance indicator as the optimisation progresses. The specific strain energy is not intended to convey any particular physical quantity. Instead it is used purely as a performance indicator and acts as a simplified proxy for multiple objective optimisation in this ESO strategy. The expression used for strain energy calculation is,

$$U = \int_\Gamma \frac{1}{2} t_i u_i d\Gamma \tag{19}$$

In practice, since the product $t_i u_i$ is non-zero only over elements on which a traction boundary condition has been prescribed (assuming there are no non-zero displacement constraints applied) the integral involved in Equation (19) conveniently reduces to the integral taken only over these elements.

The optimisation process terminates when the required volume fraction V/V_0 is achieved, otherwise the above steps followed in the optimisation process are repeated. Numerical experience suggests that this appears equivalent to the problem of minimisation of specific strain energy subject to this target volume fraction. This equivalence will be demonstrated in the examples presented in Section 5.

5. Examples

The validity and efficiency of the proposed optimisation method is tested against some benchmarking problems in the field of structural optimisation. The material properties used in these examples are: Poisson's ratio = 0.3, Young's modulus = 210 GPa, Yield stress = 280 MPa. Plane stress conditions are assumed with arbitrary thickness of 1 mm.

5.1. Example-1

The first example is a cantilever beam with an aspect ratio of 1.6. The structure is constrained at the top and bottom of the left edge and a load of 100 N is applied in the downward direction at the middle of the right edge. The initial geometry of the cantilever beam is shown in Figure 7(a). This example was solved with $RR_i = 0.05$. The first automatic hole insertion in a low stressed internal region occurs in iteration 5 (Figure 7(b)), and this hole then merges with the exterior boundary in iteration 9 shown in Figure 7(c). The second hole appears in iteration 27, which then evolves over the next iterations until two more holes are inserted each in iteration 28 and 32. The interior evolving boundaries merge in iteration 41 to form larger holes as shown in Figure 7(g). The hole insertion, evolution and merging

continue throughout the optimisation process which finally ends, when the target volume fraction of 0.33 is reached, with a topology shown in Figure 7(o). This figure closely resembles optimal geometries for this benchmark example in the previous works [16, 20, 31, 32, 19, 39, 40].

In the present implementation, holes merging takes place automatically and this eliminates the use of an additional mechanism as proposed in the BEM based ESO approach [16]. In the BEM and topological derivative based methods [20, 19], the structural geometry also suffers from jagged edges throughout the optimisation process. The use of these jagged edges within an optimisation process can generate artificial stress concentration regions within the structure, which can mislead the optimisation process. The occurrence of these artificial stress concentration regions can be avoided with the use of highly refined BEM meshes, but at the same time this will increase the computational cost of the optimisation process. In the proposed optimisation method, a NURBS based geometry representation completely eliminates these issues. In addition, the optimal geometry represented in a standard CAD format can be easily integrated in CAD/CAM based design processes. This demonstrates the effectiveness of the proposed method over the other LSM based methods presented to date, which lacks this essential feature of the design process.

The available LSM and BEM based optimisation methods presented in [32, 40] considered similar initial geometries as used for this example, and the optimal designs were obtained with 1500 and 2021 optimisation iterations, respectively. Although, in [32, 40] the optimisation process always starts from initial designs with pre-existing holes. However, with the proposed op-

timisation methods, the optimal design has been obtained in less than 100 iterations. This clearly indicates that the present optimisation method is computationally more efficient than other available LSM and BEM based methods. In addition, the proposed method automatically inserts holes and always starts with an initial guess design without pre-existing holes. This comparison demonstrates that the proposed method is capable of handling shape and topology optimisation at the same time, and this is a clear advantage of this approach.

The von Mises stress distributions during the optimisations process are shown in Figure 8. Comparison of these plots shows that the optimum structure is approaching towards a fully stressed design with a uniform stress distribution. The distributions of NURBS control points in the initial and final designs are shown in Figures 9(a) and 9(b) respectively. Both plots show a well defined control point distribution. The number of control points in the final geometry is considerably greater than the initial geometry, which shows excellent local control properties of the NURBS geometry, to maintain a smooth and well defined geometry.

During the optimisation process the specific strain energy performance indicator is closely monitored with respect to the volume constraint. The evolution of f_U at each iteration is shown in Figure 10. During the initial iterations the material removal rate is high, and the specific strain energy decreases rapidly during the initial 26 iterations. The peaks at iterations 27 and 76 are related to the automatic hole insertion and hole merging with the exterior boundary; these peaks continue to be observed up to the last iteration. The amplitudes of these peaks are high for a new large dimension

hole insertion, but these peaks die out through the optimisation process to reduce f_U. Finally, on termination of the optimisation process when the target volume fraction is achieved, it appears that the specific strain energy is still decreasing, suggesting that extending the optimisation process by more iterations would enable further reduction in this performance indicator if desired.

For this example we also compare the von Mises stresses used in our algorithm against the topological derivative method used by some authors as a guide to hole insertion. Allaire and Jouve [26] solve an adjoint problem to derive their topological derivative, but algorithms more appropriate to BEM-based optimisation schemes appear in [41] and [20]. We consider the approach [20], in which the topological derivative, D_T, is given as a function of the stress invariants, i.e.

$$D_T(x) = \frac{1}{1+\nu}\sigma \cdot \epsilon + \frac{3\nu - 1}{2(1-\nu^2)} tr\sigma tr\epsilon \tag{20}$$

where $tr\sigma$ and $tr\varepsilon$ represent the trace of the stress and strain tensors respectively. In order to perform our comparison, we consider the solutions at all internal points in the boundary element simulation at an arbitrary iteration; we choose iteration number 36. At this iteration, for each internal point we compute both σ_{vm} and D_T, and plot these results against each other. Figure 11 shows the results when σ_{vm}^2 is plotted against D_T, and this shows a clear linear relationship between these two indicators, suggesting that the topological derivative of [20] is approximately proportional to the square of the von Mises stress. We conclude that, at least for this iteration and for this problem, the use of the simple von Mises stress criterion to guide topological changes is equivalent to the use of the topological derivative.

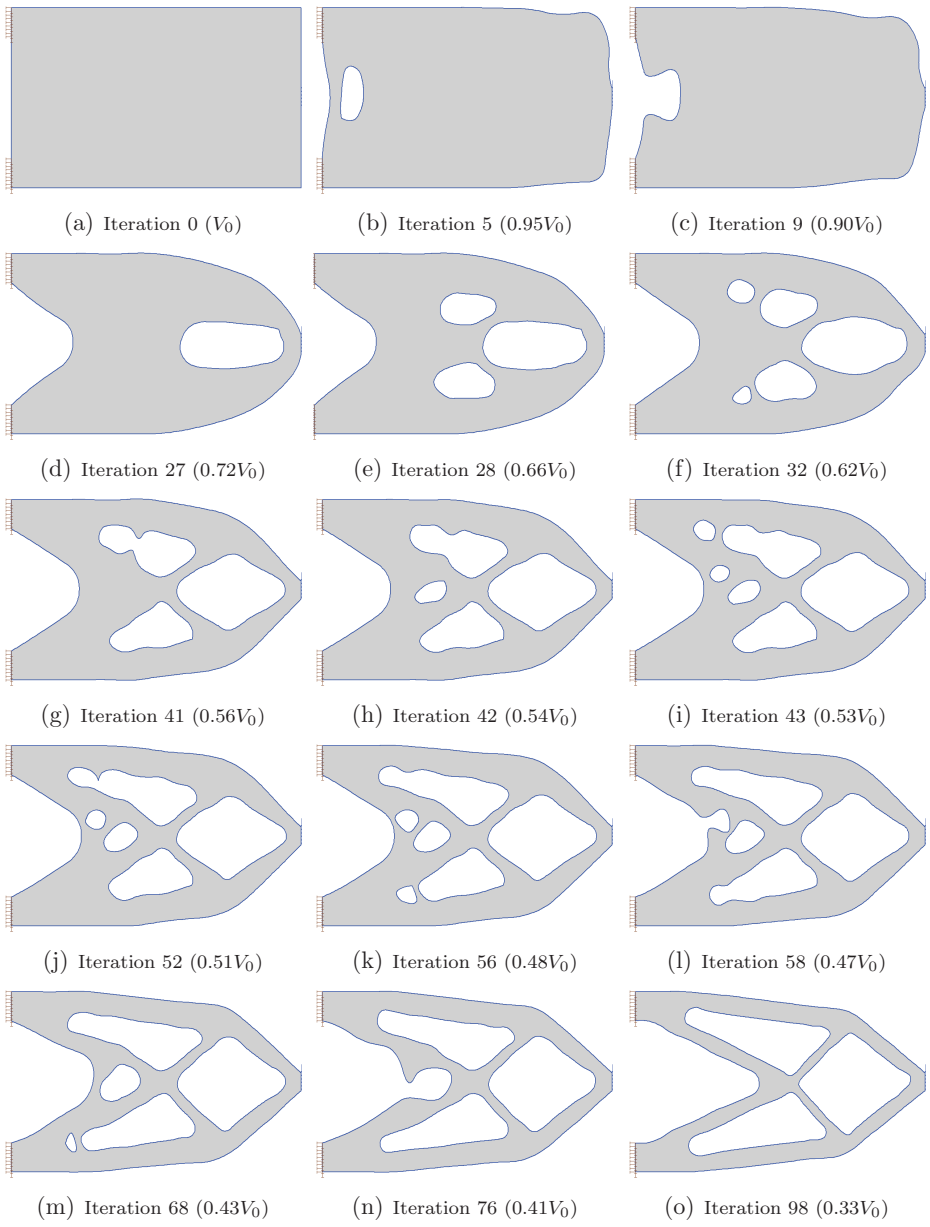

(a) Iteration 0 (V_0) (b) Iteration 5 ($0.95V_0$) (c) Iteration 9 ($0.90V_0$)

(d) Iteration 27 ($0.72V_0$) (e) Iteration 28 ($0.66V_0$) (f) Iteration 32 ($0.62V_0$)

(g) Iteration 41 ($0.56V_0$) (h) Iteration 42 ($0.54V_0$) (i) Iteration 43 ($0.53V_0$)

(j) Iteration 52 ($0.51V_0$) (k) Iteration 56 ($0.48V_0$) (l) Iteration 58 ($0.47V_0$)

(m) Iteration 68 ($0.43V_0$) (n) Iteration 76 ($0.41V_0$) (o) Iteration 98 ($0.33V_0$)

Figure 7: Structure shape and volume during optimisation

5.2. Example-2

In the second example a cantilever beam has been used with an aspect ratio of 1.5. The structure is constrained at the top and bottom of the left edge

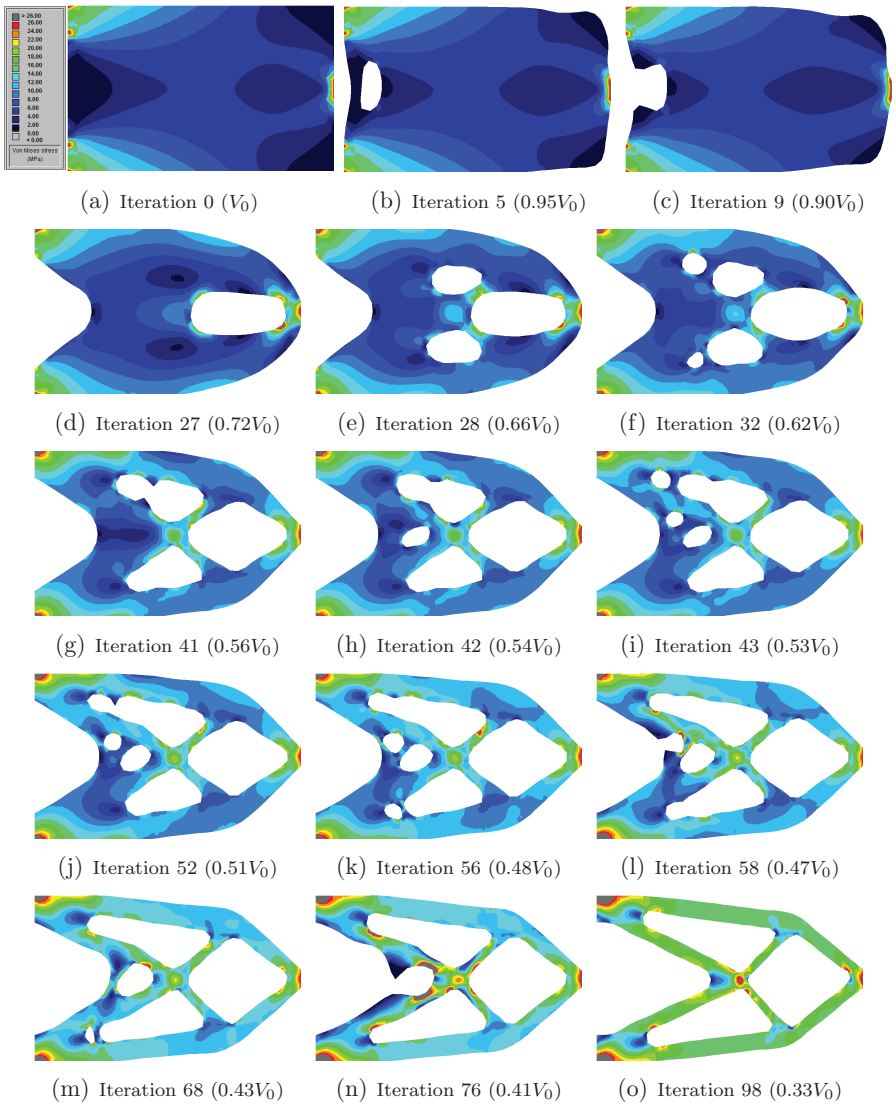

(a) Iteration 0 (V_0) (b) Iteration 5 ($0.95V_0$) (c) Iteration 9 ($0.90V_0$)

(d) Iteration 27 ($0.72V_0$) (e) Iteration 28 ($0.66V_0$) (f) Iteration 32 ($0.62V_0$)

(g) Iteration 41 ($0.56V_0$) (h) Iteration 42 ($0.54V_0$) (i) Iteration 43 ($0.53V_0$)

(j) Iteration 52 ($0.51V_0$) (k) Iteration 56 ($0.48V_0$) (l) Iteration 58 ($0.47V_0$)

(m) Iteration 68 ($0.43V_0$) (n) Iteration 76 ($0.41V_0$) (o) Iteration 98 ($0.33V_0$)

Figure 8: von Mises Stress distribution

and a load of 100 N is applied in the downward direction at the right-hand end of the bottom edge of the beam. The initial geometry, with the loading and constraints displayed, is shown in Figure 12(a). The hole insertion, evo-

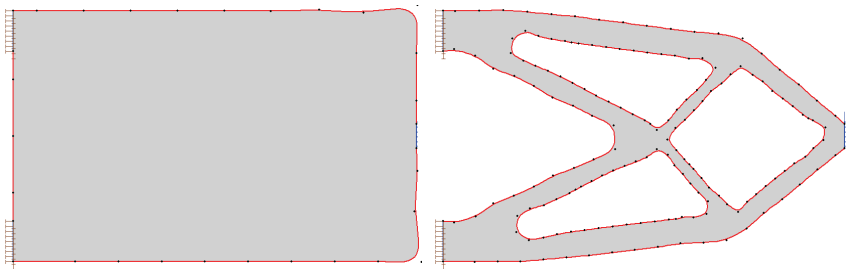

(a) Initial NURBS geometry (b) Final NURBS geometry

Figure 9: NURBS control points distribution

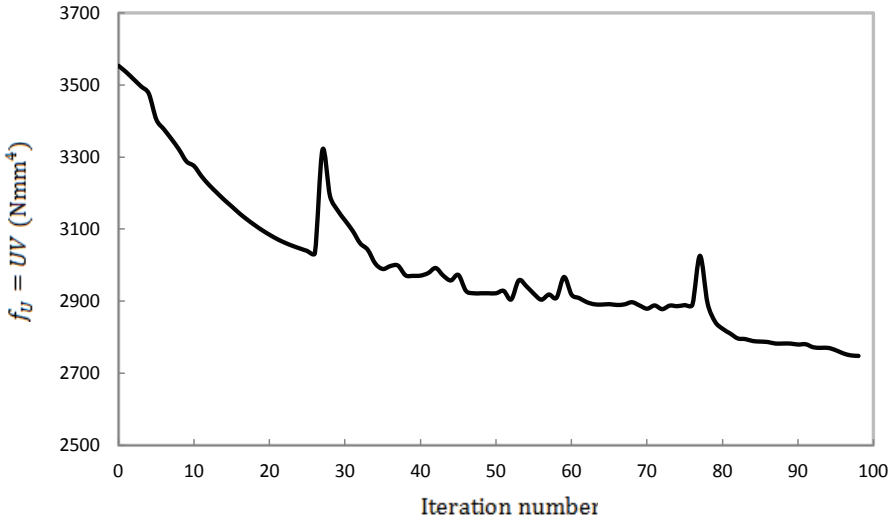

Figure 10: Specific strain energy during optimisation

lution and merging with other holes at various iterations is shown, alongside the volume at each iteration, in the collected images in Figure 12. The final optimum design closely matches those commonly presented for this benchmark example in the topology optimisation literature, i.e. [20, 19, 40, 42, 43]. Similar to the previous example, an incremental removal ratio of 0.05 is used for this problem.

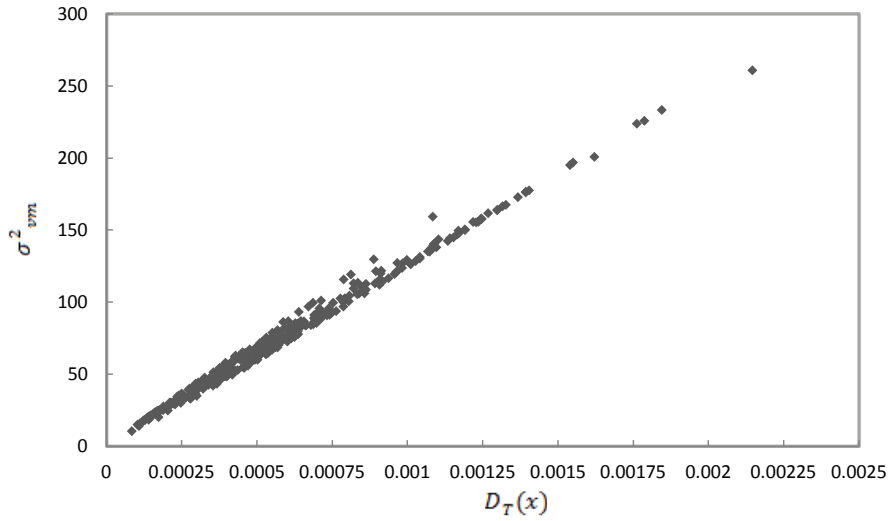

Figure 11: Comparison of σ^2_{vm} and $D_T(x)$

Similarly to the first example, the von Mises stress distribution plot in Figure 13 shows a nearly uniform von Mises stress field in the final optimum design. The control point distributions are also shown for both the initial and final designs in Figure 14.

A similar trend of specific strain energy to the previous example is observed in this example shown in Figure 15. The peaks occur when a new hole is inserted in the design and then die out after a few iterations. High peaks are observed at iterations 96 and 120 when hole merging with the boundary takes place. This effect dies out in the ensuing iterations until the required volume fraction is reached.

5.3. Example-3

The proposed method is further tested with the example of a short cantilever beam. The structure is constrained at the top and bottom of the left

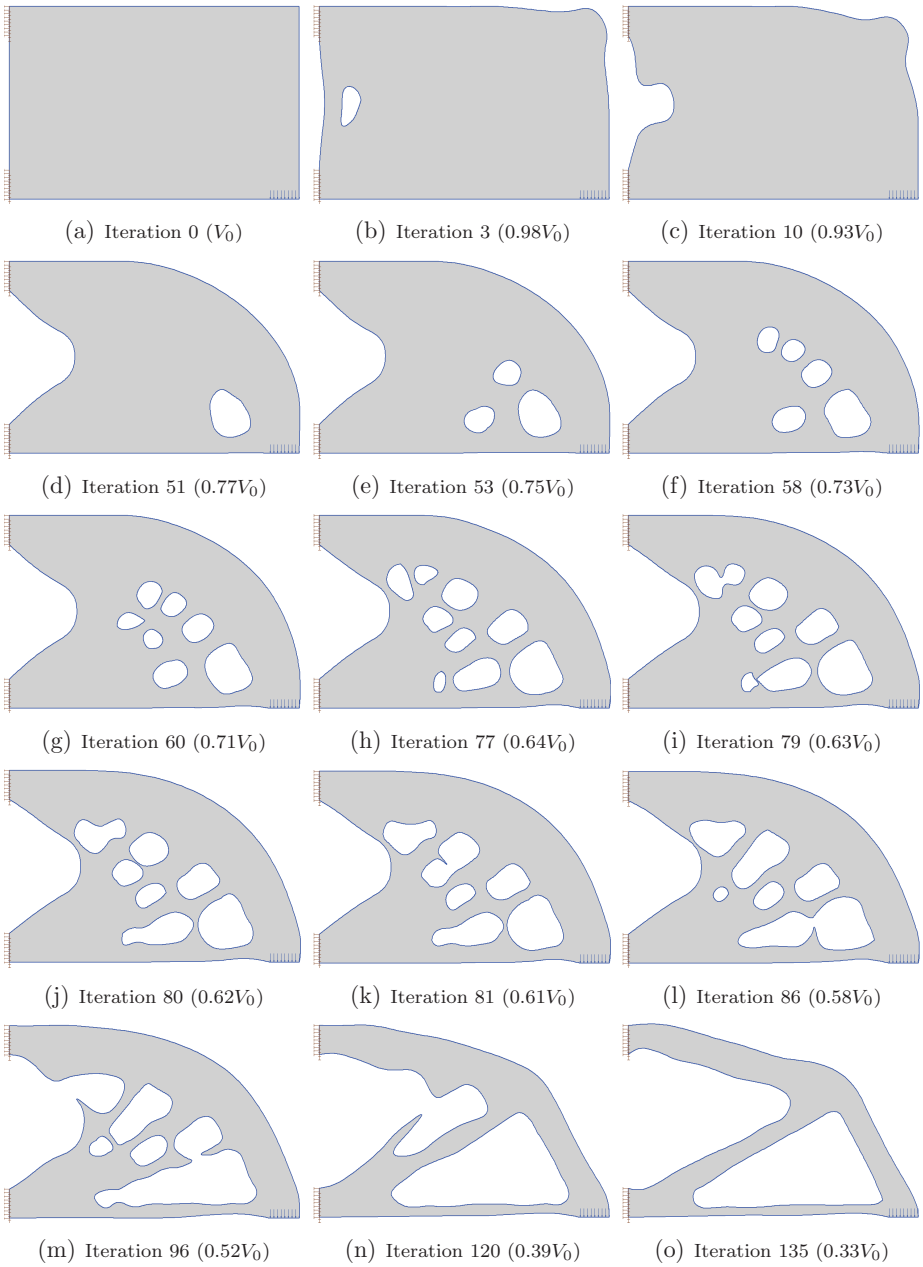

(a) Iteration 0 (V_0) (b) Iteration 3 ($0.98V_0$) (c) Iteration 10 ($0.93V_0$)

(d) Iteration 51 ($0.77V_0$) (e) Iteration 53 ($0.75V_0$) (f) Iteration 58 ($0.73V_0$)

(g) Iteration 60 ($0.71V_0$) (h) Iteration 77 ($0.64V_0$) (i) Iteration 79 ($0.63V_0$)

(j) Iteration 80 ($0.62V_0$) (k) Iteration 81 ($0.61V_0$) (l) Iteration 86 ($0.58V_0$)

(m) Iteration 96 ($0.52V_0$) (n) Iteration 120 ($0.39V_0$) (o) Iteration 135 ($0.33V_0$)

Figure 12: Structure shape and volume during optimisation

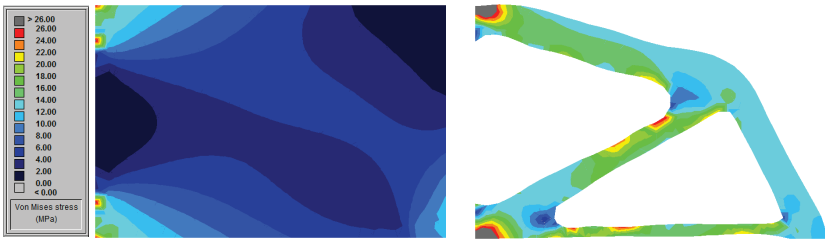

(a) Initial geometry (b) Final geometry

Figure 13: von Mises Stress distribution

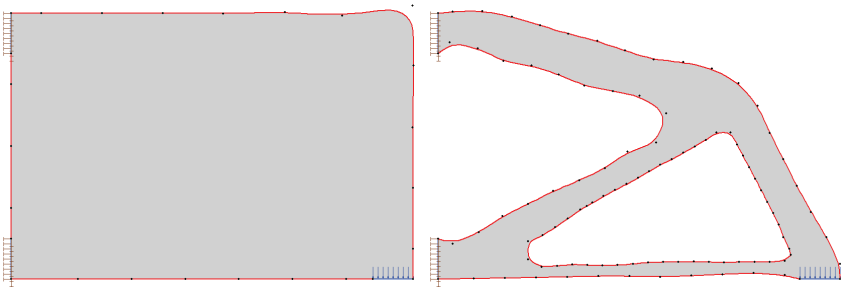

(a) Initial NURBS geometry (b) Final NURBS geometry

Figure 14: NURBS control points distribution

edge and a downward vertical load of 100N is applied at the center of the right-hand edge of the beam. Figure 16(a) shows the initial geometry with loads and constraints. The hole insertion, evolution and merging with other holes at various iterations is shown, alongside the volume at each iteration, in the collected images in Figure 16. The RR_i used in this example was 0.1.

The von Mises stress distribution plots shown in Figure 17 further validate the efficient material distribution capability of the proposed algorithm. The control points distribution in the case of short cantilever beam are shown in Figure 18 both for initial and final design. The specific strain energy

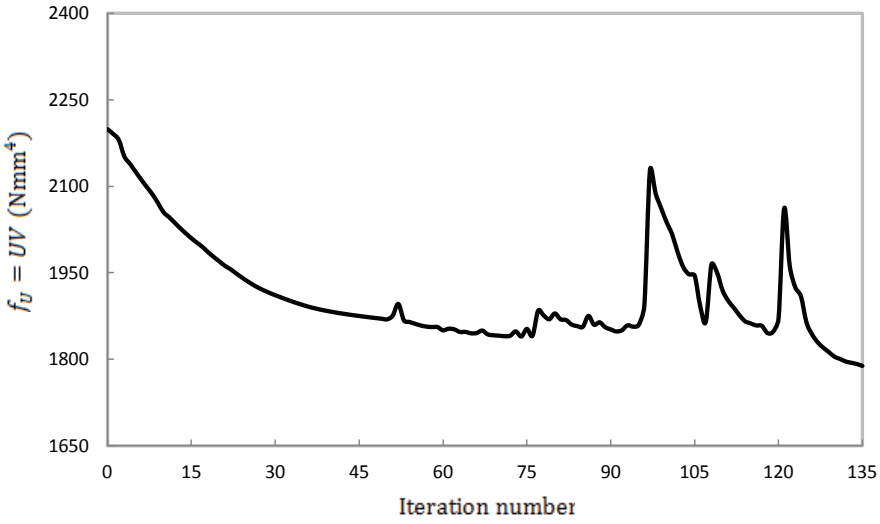

Figure 15: Specific strain energy during optimisation

evolution history is shown in Figure 19. The optimisation process terminates at iteration 50 when the final volume is 40% of the initial design. The final geometry closely matches with the optimisation results of a short cantilever beam in the literature.

5.4. Example-4

The proposed method is finally tested with the geometric model of a Michell structure. The structure with an aspect ratio of 2.0 is constrained at the left and right hand sides of the bottom edge and a vertical downward load of 100 N is applied at the middle portion of the same edge, as shown in Figure 20(a). The volume constraint for the optimal topology is set to 17% of the initial design volume. The complete topology evolution history is shown in Figure 20. The RR_i used in this example was 0.1.

Following the previous examples the von Mises stress distribution plots,

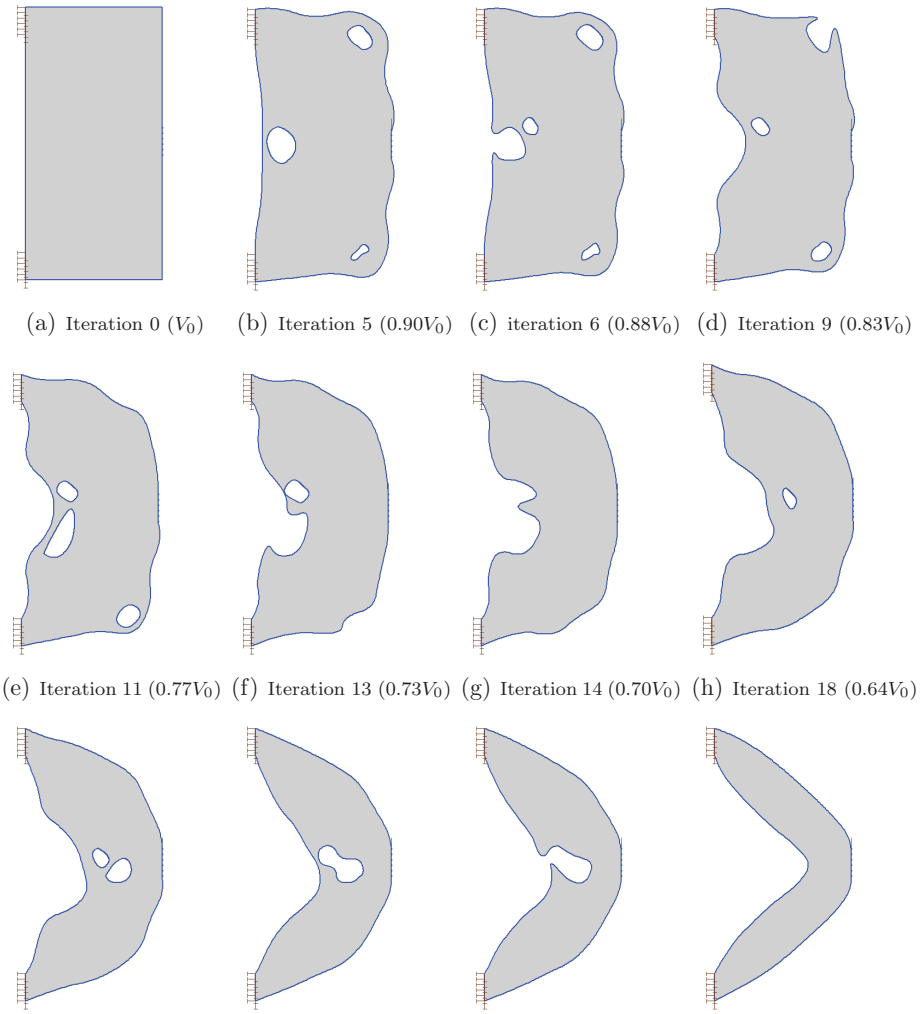

(a) Iteration 0 (V_0) (b) Iteration 5 ($0.90V_0$) (c) iteration 6 ($0.88V_0$) (d) Iteration 9 ($0.83V_0$)

(e) Iteration 11 ($0.77V_0$) (f) Iteration 13 ($0.73V_0$) (g) Iteration 14 ($0.70V_0$) (h) Iteration 18 ($0.64V_0$)

(i) Iteration 21 ($0.59V_0$) (j) Iteration 28 ($0.52V_0$) (k) Iteration 29 ($0.50V_0$) (l) Iteration 50 ($0.40V_0$)

Figure 16: Structure shape and volume during optimisation

the control points distribution and the specific strain energy evolution history are shown in Figures 21, 22 and 23, respectively.

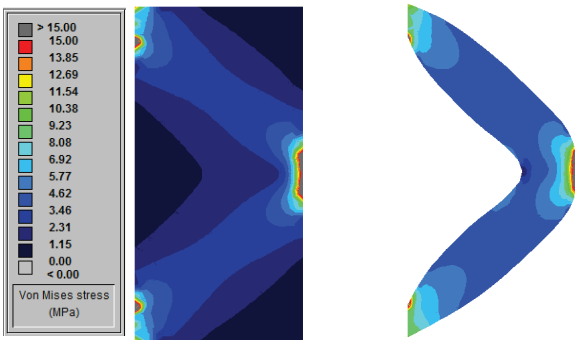

(a) Initial geometry (b) Final geometry

Figure 17: von Mises Stress distribution

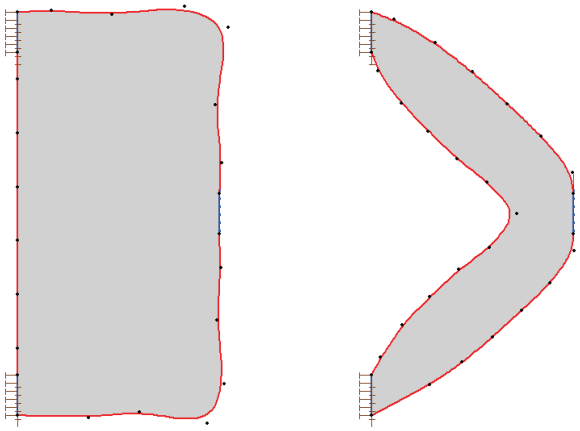

(a) Initial NURBS geometry (b) Final NURBS geometry

Figure 18: NURBS control points distribution

6. Conclusions

An evolutionary structural optimisation scheme has been presented, that uses the Level Set Method to control the evolving design geometry. At each iteration, NURBS are fitted to a set of points lying on the zero level set contour, and these are automatically meshed with boundary elements. The

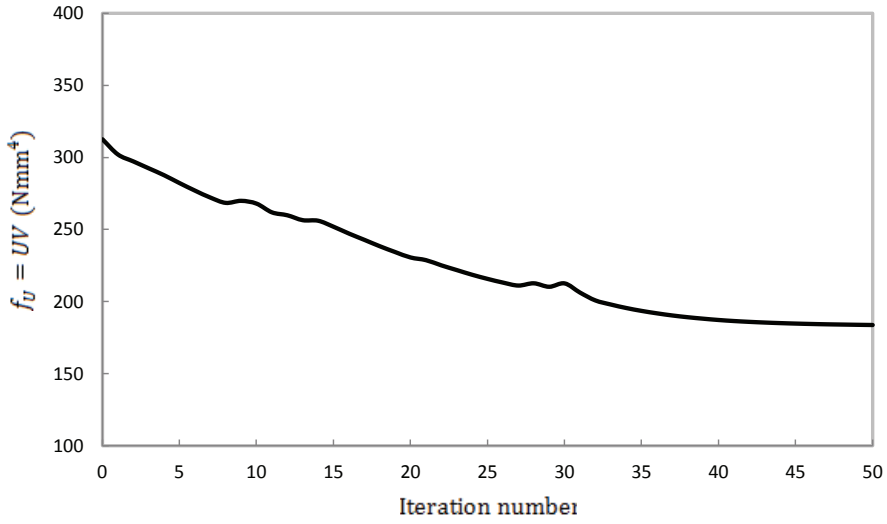

Figure 19: Specific strain energy during optimisation

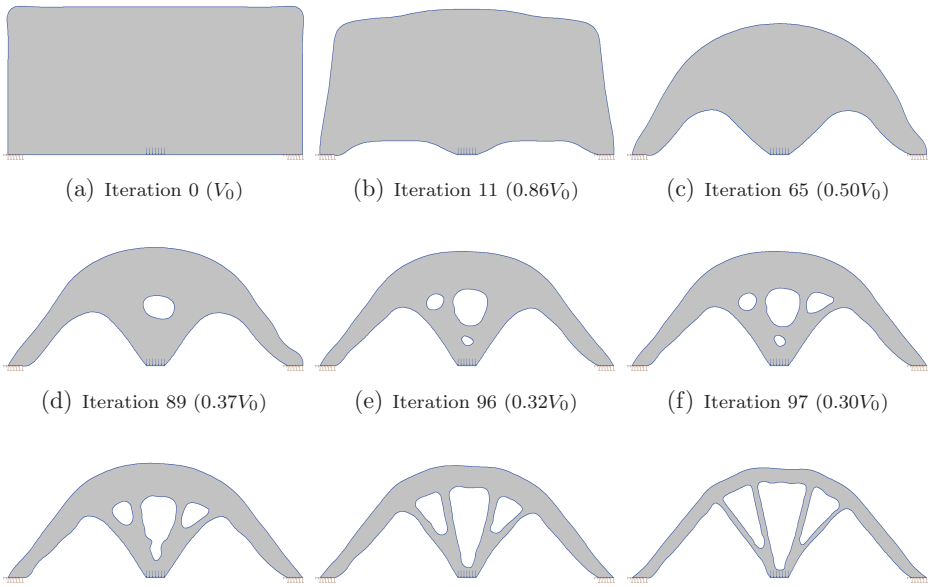

(a) Iteration 0 (V_0) (b) Iteration 11 ($0.86V_0$) (c) Iteration 65 ($0.50V_0$)

(d) Iteration 89 ($0.37V_0$) (e) Iteration 96 ($0.32V_0$) (f) Iteration 97 ($0.30V_0$)

(g) Iteration 102 ($0.28V_0$) (h) Iteration 120 ($0.23V_0$) (i) Iteration 146 ($0.17V_0$)

Figure 20: Structure shape and volume during optimisation

(a) Initial geometry (b) Final geometry

Figure 21: von Mises Stress distribution

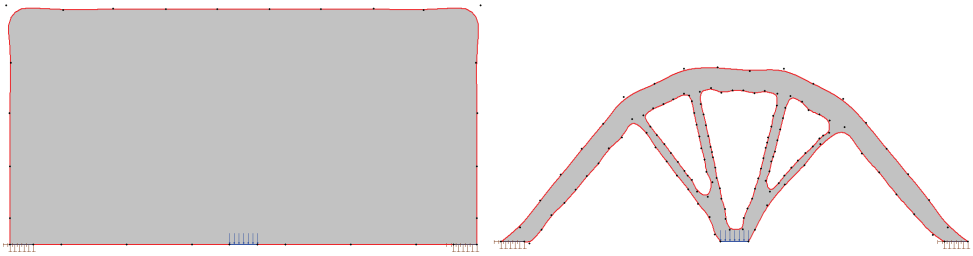

(a) Initial NURBS geometry (b) Final NURBS geometry

Figure 22: NURBS control points distribution

von Mises stress results from the BEM linear elastic simulation are mapped to a distribution of the level set velocity function, which is then used to update the design geometry in preparation for the next iteration.

The optimal design topologies and geometries obtained from the proposed method closely resemble the optima published for a range of benchmark examples in the field of structural optimisation. The method overcomes the deficiency of the traditional level set based optimisation methods which are dependent on an initial guess topology with pre-existing holes. The unique combination of BEM, evolutionary approach, LSM and NURBS provides an optimisation technique with fast and accurate structural analysis, automatic insertion and merging of holes and with the added advantage of a smooth ge-

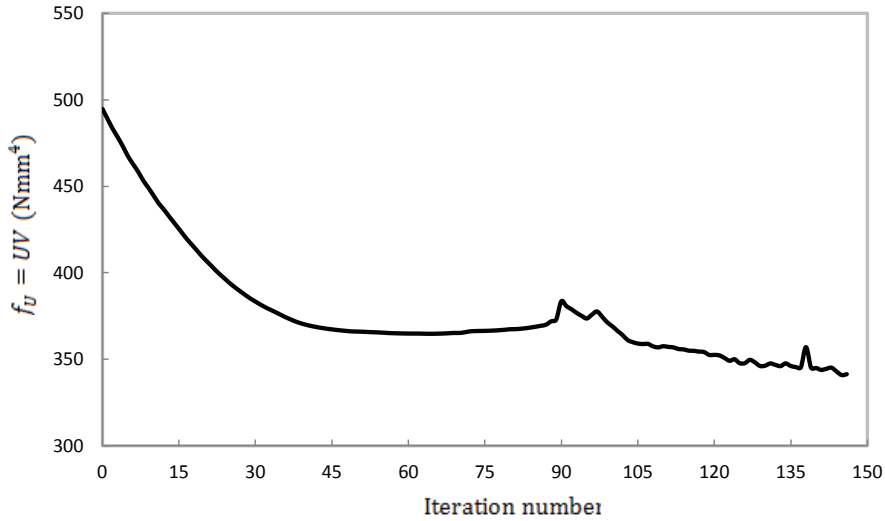

Figure 23: Specific strain energy during optimisation

ometry both from the structural analysis as well as the manufacturing point of view. It was observed that during the optimisation iterations some of the results appeared to be asymmetric when the problem was symmetric. This is due to the fact that the hole insertion is based on the internal point distribution and in the present work there is some randomness in the algorithm that distributes these internal points in the design domain. This initial study is based on the BEM, LSM and NURBS with evolutionary approach as an optimisation technique. It has been demonstrated that there is an equivalence between stress-based ESO and the use of topological derivatives to guide hole insertion algorithms. Further research work is in progress to study the above combination with other optimisation techniques.

Acknowledgements

The first author acknowledges with thanks the financial support through the Durham Doctoral Studentship scheme of Durham University.

References

[1] M. Bendsøe, N. Kikuchi, Generating optimal topologies in structural design using a homogenization method, Comput Methods Appl Mech Eng 71 (2) (1988) 197–224.

[2] G. Rozvany, M. Zhou, T. Birker, Generalized shape optimization without homogenization, Struct Multidiscip Optim 4 (3) (1992) 250–252.

[3] H. Eschenauer, V. Kobelev, A. Schumacher, Bubble method for topology and shape optimization of structures, Struct Multidiscip Optim 8 (1) (1994) 42–51.

[4] K. Maute, E. Ramm, Adaptive topology optimization, Struct Multidiscip Optim 10 (2) (1995) 100–112.

[5] P. Papalambros, M. Chirehdast, An integrated environment for structural configuration design, J Eng Design 1 (1) (1990) 73–96.

[6] Y. Xie, G. Steven, A simple evolutionary procedure for structural optimization, Comput Struct 49 (5) (1993) 885–896.

[7] O. Querin, G. Steven, Y. Xie, Evolutionary structural optimisation (ESO) using a bidirectional algorithm, Eng Comput: Int J for Comput-Aided Eng 15 (8) (1998) 1031–1048.

[8] X. Huang, Y. M. Xie, Evolutionary Topology Optimization of Continuum Structures: Methods and Applications, New York: John Wiley & Sons, 2010.

[9] M. Garcia, G. Steven, Fixed grid finite elements in elasticity problems, Eng Comput: Int J Comput-Aided Eng 16 (2) (1999) 145–164.

[10] P. Dunning, H. Kim, G. Mullineux, Introducing loading uncertainty in topology optimization, AIAA J 49 (2011) 760–768.

[11] Q. Li, G. Steven, Y. Xie, On equivalence between stress criterion and stiffness criterion in evolutionary structural optimization, Struct Multidiscip Optim 18 (1) (1999) 67–73.

[12] R. Haftka, R. Grandhi, Structural shape optimization–A survey, Comput Methods Appl Mech Eng 57 (1) (1986) 91–106.

[13] C. Soares, H. Rodrigues, L. Faria, E. Haug, Optimization of the geometry of shafts using boundary elements, J Mech Transm Autom Des 106 (1984) 199–202.

[14] J. Choi, B. Kwak, Boundary integral equation method for shape optimization of elastic structures, Int J Numer Methods Eng 26 (7) (1988) 1579–1595.

[15] K. Yamazaki, J. Sakamoto, M. Kitano, An efficient shape optimization technique of a two-dimensional body based on the boundary element method, Comput Struct 48 (6) (1993) 1073–1081.

[16] E. Cervera, J. Trevelyan, Evolutionary structural optimisation based on boundary representation of NURBS. Part I: 2D algorithms, Comput Struct 83 (23) (2005) 1902–1916.

[17] E. Cervera, J. Trevelyan, Evolutionary structural optimisation based on boundary representation of NURBS. Part II: 3D algorithms, Comput Struct 83 (23) (2005) 1917–1929.

[18] D. F. Rogers, An Introduction to NURBS: With Historical Perspective, Morgan Kaufmann, 2001.

[19] R. José Marczak, Topology optimization and boundary elements: A preliminary implementation for linear heat transfer, Eng Anal Bound Elem 31 (9) (2007) 793–802.

[20] L. Carretero Neches, A. Cisilino, Topology optimization of 2D elastic structures using boundary elements, Eng Anal Bound Elem 32 (7) (2008) 533–544.

[21] C. Bertsch, A. Cisilino, N. Calvo, Topology optimization of three-dimensional load-bearing structures using boundary elements, Adv Eng Softw 41 (5) (2010) 694–704.

[22] S. Osher, J. Sethian, Front propagating with curvature-dependent speed: algorithms based on Hamilton-Jacobi formulations, J Comput Phys 79 (1) (1988) 12–49.

[23] J. Sethian, A. Wiegmann, Structural boundary design via level set and immersed interface methods, J Comput Phys 163 (2) (2000) 489–528.

[24] M. Wang, X. Wang, D. Guo, A level set method for structural topology optimization, Comput Methods Appl Mech Eng 192 (1-2) (2003) 227–246.

[25] G. Allaire, F. Jouve, A. Toader, Structural optimization using sensitivity analysis and a level-set method, J Comput Phys 194 (1) (2004) 363–393.

[26] G. Allaire, F. Jouve, Minimum stress optimal design with the level set method, Eng Anal Bound Elem 32 (11) (2008) 909–918.

[27] S. Y. Wang, K. M. Lim, B. C. Khoo, M. Y. Wang, An extended level set method for shape and topology optimization, J Comput Phys 221 (1) (2007) 395–421.

[28] J. Luo, Z. Luo, L. Chen, L. Tong, M. Y. Wang, A semi-implicit level set method for structural shape and topology optimization, J Comput Phys 227 (11) (2008) 5561–5581.

[29] T. Yamada, K. Izui, S. Nishiwaki, A. Takezawa, A topology optimization method based on the level set method incorporating a fictitious interface energy, Comput Methods Appl Mech Eng 199 (45-48) (2010) 2876–2891.

[30] P. Wei, M. Wang, Piecewise constant level set method for structural topology optimization, Int J Numer Methods Eng 78 (4) (2009) 379–402.

[31] H. Jia, H. Beom, Y. Wang, S. Lin, B. Liu, Evolutionary level set method for structural topology optimization, Comput Struct 89 (5-6) (2011) 445–454.

[32] K. Abe, S. Kazama, K. Koro, A boundary element approach for topology optimization problem using the level set method, Commun Numer Methods Eng 23 (5) (2007) 405–416.

[33] J. Trevelyan, Concept Analyst. [Online] .www.conceptanalyst.com (2006). [link].
URL `www.conceptanalyst.com`

[34] A. Becker, The Bondary Element Methods in Engineering: A complete course, McGRAW - HILL BOOK COMPANY, 1992.

[35] D. Adalsteinsson, J. Sethian, The fast construction of extension velocities in level set methods, J Comput Phys 148 (1) (1999) 2–22.

[36] D. Adalsteinsson, J. Sethian, A fast level set method for propagating interfaces, J Comput Phys 118 (2) (1995) 269–277.

[37] J. A. Sethian, Level Set Methods and Fast Marching Methods: Evolving Interfaces in Computational Geometry, Fluid Mechanics, Computer Vision, and Materials Science, Cambridge University Press, 1999.

[38] G. Steven, L. Qing, K. Proos, Y. Xie, The role of physical sensitivity in evolutionary topology design optimisation with multi-criteria and multi-physics, in: Proceedings of the Fifth World Congress on Computational Mechanics (WCCM V). Vienna, Austria., 2002.

[39] J. H. Rong, Q. Q. Liang, A level set method for topology optimization of continuum structures with bounded design domains, Computer Methods in Applied Mechanics and Engineering 197 (17-18) (2008) 1447–1465.

[40] S. Yamasaki, T. Yamada, T. Matsumoto, An immersed boundary element method for level-set based topology optimization, International Journal for Numerical Methods in Engineering 93 (9) (2013) 960–988.

[41] A. Novotny, R. Feijóo, E. Taroco, C. Padra, Topological sensitivity analysis, Comput Methods Appl Mech Eng 192 (7) (2003) 803–829.

[42] Z. Liu, J. Korvink, R. Huang, Structure topology optimization: fully coupled level set method via FEMLAB, Structural and Multidisciplinary Optimization 29 (6) (2005) 407–417.

[43] M. Yulin, W. Xiaoming, A level set method for structural topology optimization and its applications, Advances in Engineering Software 35 (7) (2004) 415–441.